

Gradient and Texture Analysis for the Classification of Mammographic Masses

Naga R. Mudigonda, Rangaraj M. Rangayyan*, and J. E. Leo Desautels

Abstract—Computer-aided classification of benign and malignant masses on mammograms is attempted in this study by computing gradient-based and texture-based features. Features computed based on gray-level co-occurrence matrices (GCMs) are used to evaluate the effectiveness of textural information possessed by mass regions in comparison with the textural information present in mass margins. A method involving polygonal modeling of boundaries is proposed for the extraction of a ribbon of pixels across mass margins. Two gradient-based features are developed to estimate the sharpness of mass boundaries in the ribbons of pixels extracted from their margins. A total of 54 images (28 benign and 26 malignant) containing 39 images from the Mammographic Image Analysis Society (MIAS) database and 15 images from a local database are analyzed. The best benign versus malignant classification of 82.1%, with an area (A_z) of 0.85 under the receiver operating characteristics (ROC) curve, was obtained with the images from the MIAS database by using GCM-based texture features computed from mass margins. The classification method used is based on posterior probabilities computed from Mahalanobis distances. The corresponding accuracy using jack-knife classification was observed to be 74.4%, with $A_z = 0.67$. Gradient-based features achieved $A_z = 0.6$ on the MIAS database and $A_z = 0.76$ on the combined database. The corresponding values obtained using jack-knife classification were observed to be 0.52 and 0.73 for the MIAS and combined databases, respectively.

Index Terms—Acutance, breast cancer, breast masses, gradient analysis, mammography, texture, tumor classification.

I. INTRODUCTION

MAMMOGRAPHIC screening is widely used for early diagnosis of breast cancer. Recent studies have shown that mammography is sensitive in screening and diagnosis of breast cancer, but with a high false-positive rate [1]. Considering the traumatic nature and cost of biopsy, it is desirable to develop computer-based methods to distinguish accurately between benign masses and malignant tumors. Such methods may help in performing initial screening or second reading of

mammograms, and may lend objective tools to help radiologists in analyzing difficult cases and in deciding on biopsy recommendations. It is known that a small but significant number of cancer cases detected in screening programs have prompts visible in earlier screening examinations [2]. These cases represent screening errors or limitations, and may occur due to lack of an adequate understanding of perceptual features of breast abnormalities as apparent on mammograms.

Most benign masses possess well-defined and sharp boundaries, in contrast to fuzzy or ill-defined boundaries possessed by malignant tumors. However, certain benign entities such as fibroadenomas and cystic masses may also have poorly defined margins [3]. Further, benign masses are typically perceived to be more homogeneous as compared to malignant tumors in terms of density distribution. Most of the reported computer-aided analysis methods attempt to quantify the above notions to distinguish between benign masses and malignant tumors.

In a recent study on the classification of breast masses, we formulated shape-based features representing the concavity and convexity portions of a mass boundary, and the degree of spiculation possessed by the spicules present in the boundary [4], [5]. While such shape-based measures are effective in separating circumscribed benign masses from spiculated malignant tumors, they fail to distinguish between benign and malignant cases possessing similar shapes: it is known that some benign masses appear with irregular and spiculated boundaries and that some malignant tumors have rounded or simple shapes. Moreover, mammographic mass boundaries are usually blurry, making it difficult for automated detection schemes to detect precisely the mass boundaries. For these reasons, features quantifying the gradient and textural information contained by masses are needed to perform classification independent of shape.

In the present study, we focus on the development of gradient-based features and texture measures based on gray-level co-occurrence matrices (GCMs) for the classification of mammographic masses as benign or malignant. The objectives are as follows.

- 1) To investigate the significance of textural information present in mass regions [regions of interest (ROIs)] as compared to the same information present in the mass margins in terms of their benign versus malignant discriminant capabilities.
- 2) To analyze the sharpness information present in the margins of benign masses and malignant tumors by computing gradient-based measures.
- 3) To evaluate the effectiveness of a combination of gradient-based and texture-based measures in the classification of breast masses as benign or malignant.

Manuscript received June 11, 1999; revised May 11, 2000. This work was supported in part by the Alberta Heritage Foundation for Medical Research, in part by the Natural Sciences and Engineering Research Council (NSERC) of Canada, and in part by the Biomedical Engineering Graduate Programme of the University of Calgary. The Associate Editor responsible for coordinating the review of this paper and recommending its publication was L. P. Clark. *Asterisk indicates corresponding author.*

N. R. Mudigonda is with the Department of Electrical and Computer Engineering, University of Calgary, Calgary, AB, Canada T2N 1N4.

*R. M. Rangayyan is with the Department of Electrical and Computer Engineering, and the Department of Radiology, University of Calgary, Calgary, AB, Canada T2N 1N4 (e-mail: ranga@enel.ucalgary.ca).

J. E. L. Desautels is with the Department of Electrical and Computer Engineering, University of Calgary, Calgary, AB, Canada T2N 1N4. He is also with the Alberta Cancer Board, Calgary, AB, Canada T2P 3G9.

Publisher Item Identifier S 0278-0062(00)08641-9.

The contents of the paper are organized as follows. Section II presents a detailed review of the literature concerning gradient and texture analysis for discrimination of mammographic masses. Section III explains the methods proposed to facilitate the extraction of a ribbon of pixels across a mass boundary to compute gradient-based and GCM-based texture measures. Section IV describes the gradient-based features and GCM-based texture measures used in the pattern classification experiments. Section V contains the details of the image database, and Section VI describes the results of the pattern classification experiments.

II. GRADIENT AND TEXTURE ANALYSIS OF MAMMOGRAPHIC IMAGES

In addition to textural changes caused by microcalcifications, the presence of spicules arising from masses causes disturbances in the homogeneity of tissues, and may result in architectural distortion in the surrounding breast parenchyma. As a result, many studies have focused on quantifying the textural content in the mass ROI and mass margins.

Kimme *et al.* [6] proposed an automatic procedure for the detection of suspicious abnormalities on xeromammograms by identifying breast tissues and partitioning them into at most 144 sections per image. Ten normalized statistics for each section were used as texture features, and classification of 2270 mammographic sections of eight patients with six best-performing features yielded a false positive rate of 26% and a false negative rate of 0.6%. Petrosian *et al.* [7] investigated the usefulness of texture features based on spatial gray-level dependence (SGLD) matrices for the classification of masses and normal tissues. With a dataset of 135 ROIs, the methods indicated 89% sensitivity and 76% specificity in the training step, and 76% sensitivity and 64% specificity in the test step using the leave-one-out method.

Chan *et al.* [8] investigated the effectiveness of texture features derived from SGLD matrices for differentiating masses from normal breast tissue in digitized mammograms. One-hundred-sixty-eight ROIs with masses and 504 normal ROIs were examined, and eight features including correlation, entropy, energy, inertia, inverse difference moment, sum average moment, sum entropy, and difference entropy were calculated for each region. Their method resulted in an area under the receiver operating characteristics (ROC) curve of 0.84 for the training set and 0.82 for a test set. Kinoshita *et al.* [9] used a combination of shape and texture features based on GCMs. Using a three-layer feed-forward neural network, they reported 81% accuracy in the classification of benign and malignant breast lesions with a dataset of 38 malignant and 54 benign lesions.

Analysis of gradient or transition information present in the boundaries of masses has been attempted by a few researchers in order to arrive at benign/malignant decisions. Huo *et al.* [10] extracted mass regions using region growing methods, and proposed two spiculation measures based on the analysis of radial edge-gradient information in the periphery of the extracted regions. Classification studies performed using the features yielded an area of 0.85 under the ROC curve. Kok *et al.* [11] used texture features, fractal measures, and

edge-strength measures computed from suspicious regions for lesion detection.

Guliatto *et al.* [12] proposed a fuzzy region growing method for segmenting breast masses. The method has been reported to depict the transition information present around tumor boundaries in mammographic images. Statistical measures computed from the fuzzy membership values in bounding ribbons enclosing the resulting regions have shown the potential to classify masses and tumors as benign or malignant. Rangayyan *et al.* [13] proposed a region-based edge profile acutance measure for evaluating the sharpness of mass boundaries and achieved a benign/malignant classification accuracy of 92% on a dataset of 54 images consisting of 28 benign and 26 malignant cases. Problems associated with the acutance measure are discussed in the section on feature extraction and modifications are proposed.

Many automated breast mass segmentation algorithms have used texture measures in the detection procedure to differentiate masses from normal breast parenchyma in order to reduce the number of false-positives. Kegelmeyer [14] developed a method to detect stellate lesions in mammograms and computed Laws texture features from a map of local edge orientations. A binary decision tree was used to classify the features. Detection results with five test images yielded a sensitivity of 83% with 0.6 false-findings per image. Groshong and Kegelmeyer [15] used the circle Hough transform for the detection of circumscribed lesions by extending the dense feature map principles of their earlier study on the detection of spiculated lesions. Kobatake *et al.* [16] used the iris filter for the detection of approximately rounded convex regions. Texture features based on GCMs of the iris filter's output coupled with four features derived based on the histogram of the mass ROI were used to isolate malignant masses from normal tissue. The methods resulted in a detection sensitivity of 88% with 1.34 false positives per image with a dataset of 241 malignant tumors. Petrick *et al.* [17] proposed an adaptive density-weighted contrast enhancement filter in conjunction with a Laplacian-of-Gaussian edge detector for the detection of masses. A set of texture features based on GCMs yielded a true-positive detection rate of 80% at 2.3 false positives per image with a dataset of 168 cases.

Polakowski *et al.* [18] developed a model-based vision algorithm using difference-of-Gaussian filters to detect masses and computed nine features based on size, circularity, contrast, and Laws texture features. A multilayer perceptron neural network was used for the classification of breast masses as benign or malignant. With a dataset of 36 malignant and 53 benign cases, they reported a detection sensitivity of 92% for identifying malignant masses, with 1.8 false positives per image. Brzakovic *et al.* [19] proposed an automated detection and Bayesian classification scheme using tumor size, shape, and intensity changes in extracted regions. Lau and Bischof [20] applied a transformation based on the outline of the breast to identify asymmetries in breast architecture. Using a B-spline model of the breast outline to normalize images, they compared features including brightness, roughness, and directionality to define asymmetry measures for breast tumor detection.

Researchers have also used fractal measures for the detection and characterization of lesions. Priebe *et al.* [21] used texture

and fractal features for the detection of developing abnormalities. Burdett *et al.* [22] used fractal measures and nonlinear filters for characterization of lesion diffusion.

Many studies have focused on transforming the space-domain intensities into some other forms for analyzing gradient and texture information. Claridge and Richter [23] developed a Gaussian blur model to characterize the transitional information in the boundaries of mammographic lesions. For analyzing the blur in the boundaries and to determine the prevailing direction of linear patterns, a polar coordinate transform (PCT) was applied to map the lesion into polar coordinates. A measure of spiculation was computed from the PCT images to discriminate between circumscribed and spiculated lesions as the ratio of the sum of vertical gradient magnitudes to the sum of horizontal gradient magnitudes.

Sahiner *et al.* [24] introduced the rubber-band straightening transform (RBST) for classifying mammographic masses as malignant or benign. The RBST method transforms a band of pixels surrounding the boundary of a segmented mass onto the Cartesian plane. The band of pixels is extracted in the perpendicular direction from every point on the boundary. Texture features based on SGLD matrices computed from the RBST images resulted in an area of 0.94 under the ROC curve. They reported that texture analysis of RBST images yielded better benign/malignant discrimination than analysis of the original space-domain images. However, such a transformation is sensitive to the precise extraction of the band of pixels surrounding the ROI; the method may face problems with masses having highly spiculated margins.

Sameti *et al.* [25] studied the structural differences between the regions that subsequently formed malignant masses on mammograms, and other normal areas in images taken in the last screening prior to the detection of tumors. Manually identified circular ROIs were transformed into their optical density equivalents, and further divided into three discrete regions representing low, medium, and high optical density values. Based on the discrete regions, a set of photometric and texture features were extracted. They reported that in 72% of the 58 breast cancer cases studied, it was possible to realize the differences between malignant mass regions and normal tissues in previous screening images.

Chitre *et al.* [26] used texture measures for the classification of microcalcification regions on mammograms as benign or malignant. Such works will not be reviewed here as the focus of present study is on analyzing mass regions.

Numerous other works have focused on morphological features to classify mammographic masses. A detailed review of this topic appears in our recent papers on shape analysis of masses [4], [5].

Previous works [24] based on the analysis of texture patterns in transformed versions of images have reported very good trends in classification results. However, in the absence of an analytical basis, such transformations often remain irreversible and are vulnerable to the varying complexity of mass shapes. The resulting patterns and effects of such transformations cannot match or reflect the true textural content of the masses under analysis. Considering the above, the objectives of the present study are focused to verify the well-perceived notions of

differences in mass homogeneity and boundary sharpness in the space-domain images without resorting to any transformation. We propose to compute gradient-based and GCM-based texture features both within the mass ROIs and in ribbons or bands of pixels surrounding the mass ROIs. The ribbon of pixels defined in this paper represents the transitional information in a mass margin from the inside of the mass to its surrounding tissues, and not merely the information that is external to the mass boundary as in the method of Sahiner *et al.* [24] and Huo *et al.* [10].

III. EXTRACTION OF THE RIBBON OF PIXELS

In order to compute the gradient-based measures described in the following Section IV, it is necessary to extract pixel intensities from the inside of the mass boundary to the outside along the perpendicular direction at every point on the boundary. The extracted pixels cumulatively form the ribbon or band of pixels that we propose to analyze using GCM-based texture features. The boundaries used in the present work were manually drawn by an expert radiologist (J. E. L. Desautels), and include artificial, minor modulations that could lead to inaccuracies and problems in the estimation of the perpendicular direction at a particular point on the boundary. We, therefore, use polygonal models of the mass boundaries, computed as briefly described below, in order to approximate the boundaries with polygons of known parameters, so that the computation of the perpendiculars becomes feasible at all the boundary points. We have also developed shape-based features for the classification of mammographic masses using the polygonal models [4], [5].

Given a mass boundary as specified by the set of its x and y coordinates, the first step in our polygonal modeling algorithm is to segment the boundary into a set of prominent and piece-wise continuous curves. We achieve this by locating the points of inflection on the boundary [27], [4], [5]. We then derive a polygonal approximation of the boundary, by splitting each individual curved part into a set of linear segments based on the arc-to-chord deviation. This procedure is iterated subject to pre-specified threshold values of arc-to-chord deviation and minimum length of the resulting polygonal segments, so as to minimize the error between the true boundary length and the cumulative length computed from the polygonal segments. The details of this procedure may be found in Mudigonda *et al.* [4] and Rangayyan *et al.* [5]. In the computation of acutance, Rangayyan *et al.* [13] implemented a version of the polygonization algorithm proposed by Ventura and Chen [28] in such a manner as to require user input for the number of segments to use in the model. In contrast, the polygonal modeling technique used in the present study is totally automated and requires no user input at any stage. The technique has proven to be robust and has performed satisfactorily on highly nonlinear and irregular mass boundaries in our database [4], [5].

With the known equations of the sides of the polygonal model, it is possible to estimate the normal at every point on the boundary. Although it is possible to compute the precise orientation of the normal at every point on the boundary as above, the intensity values corresponding to fractional values that could result in the computation of coordinates of pixels in

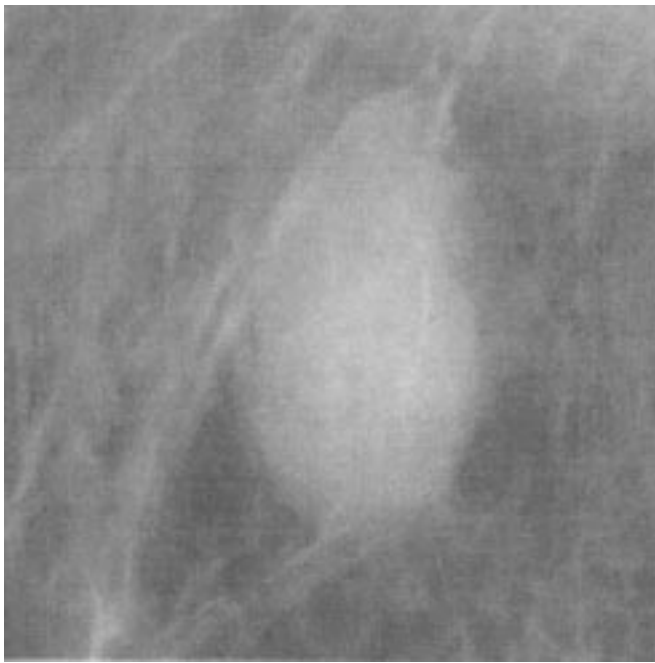


Fig. 1. A 900×1000 -pixel section of a mammogram containing a circumscribed benign mass. Pixel size = $50 \mu\text{m}$.

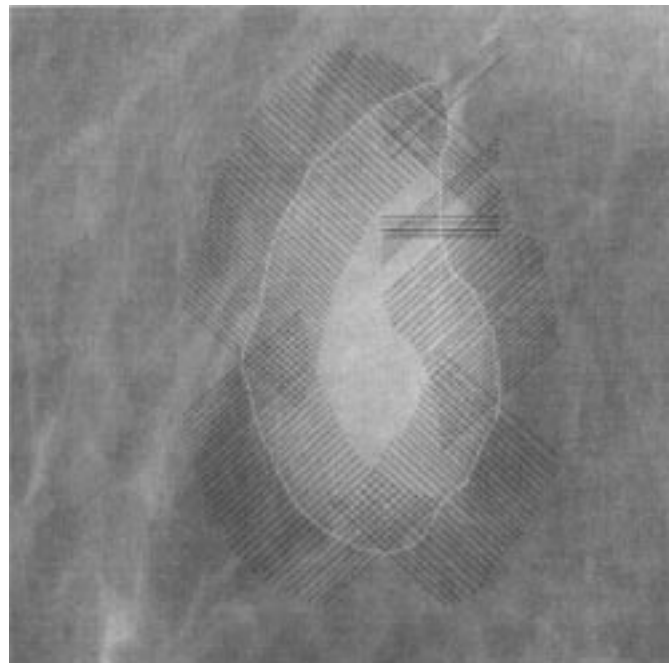


Fig. 2. Extraction of normal pixels (shown in black lines) on the boundary of the benign mass in Fig. 1. Maximum number of pixels on either side of the boundary = 80.

the normal orientation are not readily available in the image (without the use of interpolation of the intensities of neighboring pixels). This is true irrespective of the resolution of the image. Hence, in the present study, each estimated normal was mapped to the closest of the four directions (0° , 45° , 90° , and 135°) that are available as straight lines on a discrete grid. At the point of intersection of two successive sides of the polygon (a vertex of the polygonal model), the bisector of the angle formed by the intersecting linear segments was taken to be the perpendicular direction.

Fig. 1 shows a 900×1000 -pixel section of a mammogram containing a circumscribed benign mass. Figs. 2 and 3 show the normals (shown only for every tenth pixel in Fig. 2) and the extracted ribbon of maximal width of 8 mm across the boundary (4 mm or 80 pixels on either side of the boundary, where available, at a resolution of $50 \mu\text{m}$ per pixel). A similar set of images for a spiculated malignant tumor (size of each image = 560×630 pixels) is presented in Figs. 4–6.

As it can be seen from Figs. 5 and 6, the proposed method can adapt to a tumor's shape complexity: the width of the extracted ribbon at any point on the boundary is limited to a maximum of 80 pixels on either side of the boundary or the depth of the mass at that particular point. This is significant especially in the case of spiculated tumors possessing sharp spicules or microlobulations such that the extracted normals do not cross over into adjacent spicules or mass portions. In three of the 54 images analyzed in the present work, the masses are located close to the edges of the images. In these cases, the width of the ribbon of pixels was limited to the available pixels in the image at the edge locations. The ribbon width of 4 mm was determined by a radiologist specialized in mammography (J. E. L. Desautels), in order to take into account the possible depth of infiltration or diffusion of masses into the surrounding tissues. Sahiner *et al.*

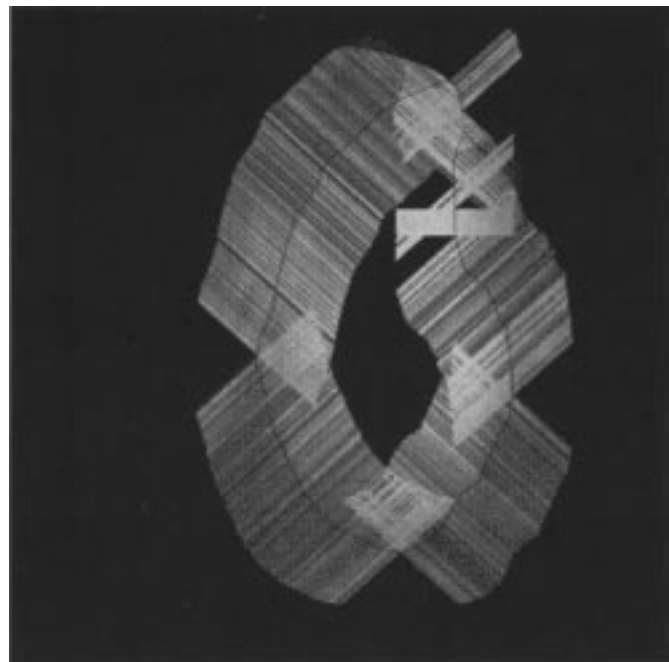


Fig. 3. Ribbon or band of pixels across the boundary of the benign mass in Fig. 1 extracted for computing gradient and texture features.

[24] also considered a boundary ribbon of width 4 mm for analyzing texture using the RBST method.

IV. FEATURE EXTRACTION

The mass regions and the ribbons of pixels extracted from the mass margins, as explained in Section III, were analyzed using gradient-based and GCM-based texture measures for use in benign/malignant pattern classification.

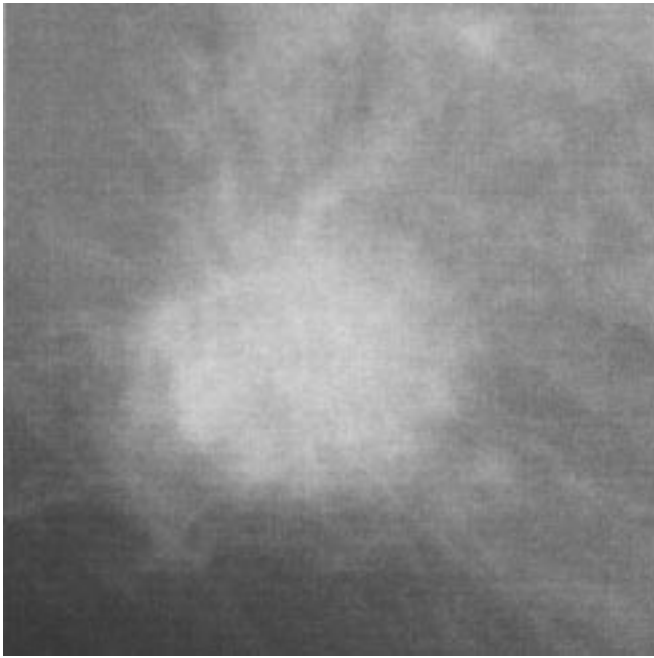


Fig. 4. A 560×630 -pixel section of a mammogram containing a spiculated malignant tumor. Pixel size = $50 \mu\text{m}$.

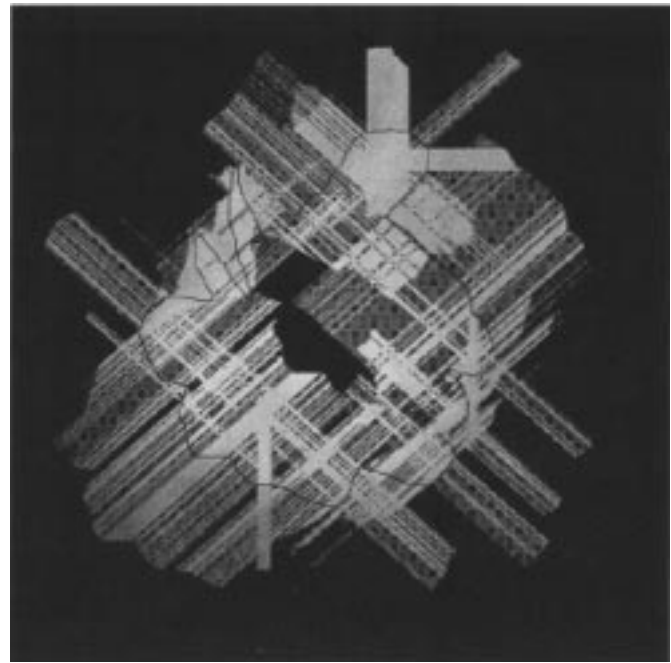


Fig. 6. Ribbon or band of pixels across the boundary of the malignant tumor in Fig. 4 extracted for computing gradient and texture features.

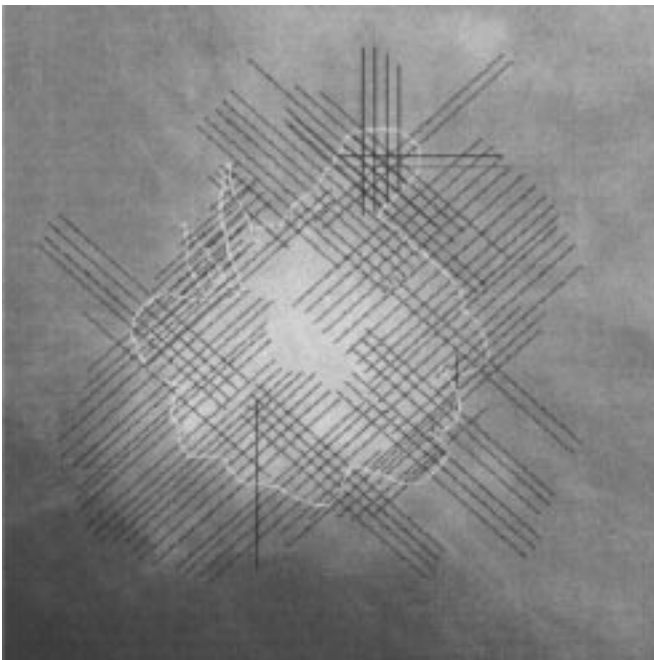


Fig. 5. Extraction of normal pixels (shown in black lines) on the boundary of the malignant tumor in Fig. 4. Maximum number of pixels on either side of the boundary = 80.

A. Gradient-Based Measures

Due to infiltration into surrounding tissues, malignant breast lesions often permeate larger areas than apparent on mammograms. As a result, mass margins in mammographic images do not reveal a clear-cut transition or gradient information. Hence, it is difficult for an automated detection procedure to realize precisely the boundaries of mammographic masses as there cannot be any objective measure of such precision. Also, when manual

segmentation is used, as is the case in the present study, there are bound to be large inter-observer variations in the location of mass boundaries due to subjective differences in notions of edge sharpness. Considering the above, it is appropriate for gradient-based measures to characterize the global gradient phenomenon in the mass margins without being sensitive to the precise location of the mass boundary. In the present study, we endeavor to develop features based on directional gradient profiles that tolerate uncertainties in the location of mass boundaries.

1) *Directional Gradient Strength*: The subjective impression of sharpness perceived by the human visual system is a function of the averaged variations in intensities between the relatively light and dark areas of an ROI. Based on this, Higgins and Jones [29] proposed a measure of acutance to compute sharpness as the mean-squared gradient along knife-edge spread functions of photographic films. Rangayyan and Elkadiki [30] extended this concept to two-dimensional ROIs in images. Later, Rangayyan *et al.* [13] used the measure to classify mammographic masses as benign or malignant: acutance was computed using directional derivatives along the perpendicular at every boundary point by considering inside-to-outside differences of intensities across the boundary normalized to unit pixel distance. The method has limitations due to the following reasons.

- Since derivatives were computed based on inside-to-outside differences across the boundary, the measure is sensitive to the actual location of the boundary. Further, it is sensitive to the number of differences (pixel pairs) that are available at a particular boundary point, which could be relatively low in sharply spiculated portions as compared to fairly circumscribed portions of a mass ROI. The measure, thus, becomes sensitive to shape complexity as well, which is not intended.

- The final acutance value for a mass ROI was obtained by normalizing the mean-squared gradient computed at all the points on the boundary with a factor dependent upon the maximum gray-level range and the maximum number of differences used in the computation of acutance. For a particular mass under consideration, this type of normalization results in large differences in acutance values for varying numbers of pixel pairs considered.
- In the computation of acutance, the number of sides of the polygon required for polygonal approximation of the boundary was manually input by visually judging the complexity of the boundary. The procedure could result in large variations in acutance values for a given boundary due to subjective limitations in perceiving the complexity of the boundary and, hence, could affect the reproducibility of results obtained.

In the present study, the above-mentioned drawbacks are addressed by developing a consolidated measure of directional gradient strength as explained below. Given the boundary of a mass formed by N points, the first step is to compute the root-mean-squared (rms) gradient in the perpendicular direction at every point on the boundary with a set of successive pixel pairs as made available by the ribbon extraction method explained in Section III. The rms gradient d_i at the i th boundary point is obtained as

$$d_i = \sqrt{\frac{\sum_{j=0}^{(n_i-1)} [f_i(j) - f_i(j+1)]^2}{n_i}} \quad (1)$$

where $f_i(j)$, $j = 0, 1, 2, \dots, n_i$, are $(n_i + 1)$ number of pixels available along the perpendicular at the i th boundary point including the boundary point. n_i is limited to a maximum of 160 pixels (80 pixels on either side of the boundary) in this paper.

A modified measure of acutance based on directional gradient strength A_{dg} of the ROI is computed as

$$A_{dg} = \frac{1}{(f_{\max} - f_{\min})} \frac{\sum_{i=1}^N d_i}{N} \quad (2)$$

where f_{\max} and f_{\min} are the local maximum and local minimum pixel values in the ribbon of pixels extracted, and N is the number of pixels along the boundary of the ROI. Since the rms gradients computed over several pixel pairs at each boundary point are used in the computation of A_{dg} , the measure is expected to be stable in the presence of noise, and is further expected to be not sensitive to the actual location of the boundary. Also, A_{dg} is not affected by the varying number of normal pixels at different points on the boundary that are adaptively extracted depending on the complexity of the boundary. The denominator $(f_{\max} - f_{\min})$ in (2) serves as an additional normalization factor in order to account for the changes in gray-level contrast of images from various databases; it also normalizes the A_{dg} measure to the range (0, 1).

2) *Coefficient of Variation of Gradient Strength:* In the presence of objects with fuzzy backgrounds, as is the case in mammographic images, the mean-squared gradient as a measure of

sharpness may not result in adequate confidence intervals for the purposes of pattern classification. Hence statistical measures need to be adopted to characterize the feeble gradient variations across the mass margins. Considering this notion, we propose a feature based on the coefficient of variation of the edge strength values computed at all points on the ROI boundary. The purpose of this feature is to investigate the variability in the sharpness of a mass around its boundary, in addition to evaluating its average sharpness with the measure A_{dg} . Variance is a statistical measure of signal strength, and can be used as an edge detector as it responds to boundaries between regions of different brightness [31]. We propose to compute the variance (σ_w^2) localized in a moving window of an odd number of pixels (M) in the perpendicular direction at the boundary pixel as

$$\sigma_w^2 = \frac{1}{M} \sum_{n=[-M/2]}^{[M/2]} [f_i(n) - \mu_w]^2. \quad (3)$$

$M = 5$ in the present work; $f_i(n)$, $n = 0, 1, 2, \dots, n_i$, are the pixels considered at the i th boundary point in the perpendicular direction; and μ_w is the running mean intensity in the selected window, with

$$\mu_w = \frac{1}{M} \sum_{n=[-M/2]}^{[M/2]} f_i(n). \quad (4)$$

The window is moved over the entire range of pixels made available at a particular boundary point by the boundary ribbon extraction method discussed in Section III. The maximum of the variance values so computed is chosen as the edge strength of the boundary point being processed. The coefficient of variation (G_{cv}) of edge strength values for all the points on the boundary is then computed. The proposed measure is not sensitive to the actual location of the boundary within the selected ribbon, and is normalized so as to be applicable to a mixture of images from different databases.

As mentioned previously, the perpendicular direction estimated at every point on the boundary using the proposed polygonal model has been mapped to the closest of the four directions available on a discrete grid. The deviation of the selected normal from the true radial direction is small at points located close to the boundary, but increases on either side of the boundary with the increase in distance. On the other hand, the sharpness information that is to be assessed using the proposed features is less prominent at points located far from the boundary where the above-mentioned deviation is at its maximum. Since the proposed gradient-based measures are designed to characterize the global sharpness information present in the ribbon of pixels and are further normalized, the approximation of the orientation of the perpendiculars may not result in significant inaccuracies in the computed features. The above point, however, needs to be verified by computing features based on precise normals including suitable interpolation methods.

B. Texture Features

The physiological composition of breast tissues results in the depiction of oriented patterns in mammographic images. The

presence of microcalcifications and/or masses causes architectural distortion in the surrounding tissues. As a result, mammographic images possess textural information that could bear discriminant features. In the present study, features computed from GCMs [32] are used to investigate if the textural information present in the mass margins or ribbons is adequate for the discrimination of benign and malignant abnormalities, as compared to the same computed from the entire mass regions. A ribbon or band of pixels was extracted for each mass ROI as explained in Section III. The spatial coordinates and intensities of the extracted pixels were preserved for constructing the GCMs. The choice of Haralick's features [32] based on GCMs was made considering their proven applicability to analyze texture in objects with irregular outlines [31], as in the case of mammographic masses.

A GCM $P_d(i, j)$ reflects the distribution of the probability of occurrence of a pair of gray levels (i, j) separated by a given distance (d) . The GCMs are constructed by mapping the gray-level co-occurrence probabilities based on spatial relations of pixels in different angular directions, while scanning the image from left-to-right and top-to-bottom. Five texture measures were computed in the present work as described below. (The subscript d is not indicated in the following equations as the measures are computed for every d used.)

- *Entropy*: A measure of nonuniformity in the image or ROI or ribbon of pixels based on the probability of co-occurrence values

$$\text{Entropy} = - \sum_{i=1}^N \sum_{j=1}^N \left(\frac{P(i, j)}{R} \right) \log \left(\frac{P(i, j)}{R} \right). \quad (5)$$

- *Second Moment*: A measure of homogeneity

$$\text{Second Moment} = \sum_{i=1}^N \sum_{j=1}^N \left(\frac{P(i, j)}{R} \right)^2. \quad (6)$$

- *Difference Moment*: A measure of contrast

$$\text{Difference Moment} = \sum_{n=0}^{N-1} n^2 \sum_{i-j=n} \left(\frac{P(i, j)}{R} \right). \quad (7)$$

- *Inverse Difference Moment*: A measure of local homogeneity

$$\begin{aligned} \text{Inverse Difference Moment} \\ = \sum_{i=1}^N \sum_{j=1}^N \frac{[P(i, j)/R]}{1 + (i - j)^2}, \quad i \neq j. \end{aligned} \quad (8)$$

- *Correlation*: A measure of linear dependency of brightness.

$$\text{Correlation} = \frac{\sum_{i=1}^N \sum_{j=1}^N [ijP(i, j)/R] - \mu_x \mu_y}{\sigma_x \sigma_y}. \quad (9)$$

In the above expressions, N is the number of gray levels, equal to 256 for the images in the present study. R is equal to the total

number of pixel pairs in the ribbon or mass ROI used for the calculation of texture features in the specified angular direction. μ_x , σ_x , μ_y , and σ_y are the mean and standard deviation values of GCM values accumulated in the x and y directions, respectively. A detailed explanation of these features has been provided by Haralick [32].

In the present study, four GCMs were constructed by scanning each mass ROI or ribbon in the 0° , 45° , 90° , and 135° directions with unit pixel distance ($d = 1$). The five features described above were computed for the four GCMs, thus, resulting in a total of 20 texture features for each ROI or ribbon based on gray-level co-occurrence statistics. A pixel distance of $d = 1$ is preferred to ensure large numbers of co-occurrences derived from the ribbons of pixels extracted from mass margins. Texture features computed from GCMs constructed for larger distances ($d = 3, 5$, and 10) were found to possess a high degree of correlation (0.9 and higher) with the corresponding features computed for unit pixel distance ($d = 1$). Hence pattern classification experiments were not carried out with GCMs constructed using larger distances. It is to be noted that in the case of GCMs constructed for angles other than 0° and 90° , the actual distance considered would be $\sqrt{2}$ times the pixel resolution in the image.

V. IMAGE DATABASE

Thirty-nine mammographic images including 16 circumscribed benign, four circumscribed malignant, 12 spiculated benign, and seven spiculated malignant masses were selected from the Mammographic Image Analysis Society (MIAS, UK) database [33]. The spatial resolution of the images is $50 \mu\text{m} \times 50 \mu\text{m}$. The optical density is linear in the range 0–3.2 and quantized to 8 bits. Although most malignant tumors encountered in mammography are spiculated and a majority of the benign masses are well-circumscribed, the MIAS database has a relatively large number of spiculated benign masses.

In order to augment the numbers of the two types of malignant tumors, 15 images (containing three circumscribed and 12 spiculated tumors) from Screen Test: Alberta Program for the Early Detection of Breast Cancer, digitized at a spatial resolution of $62 \mu\text{m} \times 62 \mu\text{m}$, were added to the study. The Screen Test images were digitized to 12-bit resolution in the optical density range of 0.0 to 2.8; however, the gray-scale range was reduced to 256 levels (8 bits) in the present work to be comparable with that of the MIAS images. The Screen Test images together with the 39 images from the MIAS database increased the total number of cases analyzed to 54 (28 benign and 26 malignant), referred to as the combined database in the discussion hereafter. All diagnoses were proven by pathologic examination of resected tissue. Sections of interest of the mammographic images were displayed on a Sun SPARC Station 2 and the boundary of each mass was traced and input to the computer by an expert radiologist specialized in mammography (J. E. L. Desautels) using *XPAINT* for *X-Windows* [13].

Application of gradient-based and texture-based features on a combination of databases raises important issues and concerns related to their abilities to achieve appropriate clustering of be-

TABLE I
COMPARISON OF THE BEST CLASSIFICATION RESULTS BETWEEN MASS ROIs AND MASS MARGINS (RIBBONS OF PIXELS) USING GCM-BASED TEXTURE FEATURES FOR 39 MIAS CASES. A_z IS THE AREA UNDER THE ROC CURVE

Details	% Accuracy (jack-knife method)				% Accuracy			
	Benign	Malignant	Total	A_z	Benign	Malignant	Total	A_z
Mass region	67.9 (19/28)	63.6 (7/11)	66.7	0.63	75.0 (21/28)	72.7 (8/11)	74.4	0.71
Mass margins	78.6 (22/28)	63.6 (7/11)	74.4	0.67	82.1 (23/28)	81.8 (9/11)	82.1	0.85

nign and malignant cases. In addition to minor differences in terms of spatial resolution between the MIAS images and the Calgary cases used in the present study (50 μm and 62 μm), the two sets of images possess significant variations in contrast. Hence, in the present study, the pattern classification tests were performed initially on the MIAS cases, and later were repeated on the combined database. The classification results are recorded separately for the MIAS cases and the combined database, and discussed in detail in Section VI.

VI. RESULTS OF PATTERN CLASSIFICATION

For each mass or tumor in the database, we computed 20 texture features based on GCMs in four directions. The features were computed from both the mass ROIs and the ribbons of pixels extracted from the mass margins. Pattern classification was carried out in three parts using the Biomedical Data Processing Package (BMDP) 7M step-wise linear discriminant analysis program [34] using the forward-stepping criterion. In the first part, the effectiveness of using ribbons around mass margins as against mass ROIs in benign/malignant classification was verified using the texture measures. The second part was designed to compare the effectiveness of margin sharpness measures against texture measures. The third part evaluates the use of a combination of gradient-based and texture-based measures.

For each case, the 7M step-wise discriminant analysis program computes posterior probabilities of the case belonging to various groups based on the Mahalanobis distances of the case from the mean values of the feature vectors of the corresponding groups. The case is classified into the group with the maximum posterior probability. The classification accuracies are computed based on the number of correctly classified cases in each of the groups. The program also realizes jack-knife validation of the results based on the same methodology as described above. Variables from the given set are rank-ordered based on F-statistics computed at each step by performing one-way analysis of variance (ANOVA) test. At each step, the forward-stepping process selects the variable possessing the maximum F-value which is in excess of a pre-specified F-to-enter threshold, set at the default value of 4.0 of the 7M program in the present work. The program further computes the canonical variable, the coefficients of which are standardized by pooled within-the-group variances, as a linear combination of the variables that are selected by the forward-stepping process. In the present work, the features with the corresponding canonical coefficient values of greater than one are finally short-listed and the classification results are reported for the combination of features short-listed for both the mass regions and the mass margins.

Part I: Mass ribbons versus ROIs using GCM-based texture features.

Since the objective here is to verify the homogeneity of mass ROIs in relation to their margins as apparent on mammograms, the analysis was performed using 28 benign masses and 11 malignant tumors belonging to the MIAS database only. This was preferred to avoid the complications arising out of mixing images from different databases. Seven leading features (with canonical coefficients of greater than 1) including three measures of correlation ($d = 1$ at 0° , 45° , and 135°), two measures of difference moments ($d = 1$ at 0° and 90°), and two measures of second moments ($d = 1$ at 0° and 135°) were selected from the 20 texture features computed from the ribbons. The classification accuracy was found to be the maximum with the seven features listed. The three most-effective features selected for analyzing mass ROIs include two measures of inverse difference moments ($d = 1$ at 0° and 135°) and a measure of correlation ($d = 1$ at 135°).

Table I presents the results of pattern classification using the selected combinations of features for both mass ROIs and ribbons. The best benign/malignant classification accuracy of 82.1% with a jack-knife accuracy of 74.4% was obtained for the 39 MIAS cases by using the seven texture features (listed in the preceding paragraph) computed from ribbons of pixels across the mass boundaries. All classification accuracies quoted were obtained using the procedure in the BMDP package that estimates posterior probabilities of cases belonging to the benign and the malignant groups at a cutpoint of 0.5 for both the groups. The texture features from mass ribbons resulted in equally high sensitivity and specificity of 82%. This indicates the significance of textural information in mass margins in benign/malignant discrimination. The GCM-based texture measures computed from the whole mass ROIs yielded at best 74.4% benign/malignant classification accuracy only, with a jack-knife accuracy of 66.7% with the 39 MIAS cases.

The performance of the selected combinations of features was further validated using ROC methodology. ROC plots were obtained using the BMDP package by varying the cut-points for benign and malignant prior probabilities between zero and one in steps of 0.1. The procedure does not affect the discriminant ratings or the selection of variables and influences only the computation of the constant term in the discriminant function, thereby resulting in varying classification accuracies. The area (A_z) under the ROC curve was computed using the trapezoidal rule. The top seven GCM-based texture features computed from the mass ribbons resulted in $A_z = 0.85$, as opposed to $A_z = 0.71$ obtained by using the top three GCM-based features computed from the mass regions, as shown in Table I. The corresponding results ob-

TABLE II
NUMBER OF CASES CORRECTLY CLASSIFIED BY THE GRADIENT-BASED AND GCM-BASED TEXTURE FEATURES COMPUTED FROM MASS MARGINS (RIBBONS) FOR THE MIAS CASES

Features	% Accuracy (jack-knife method)				% Accuracy			
	Benign	Malignant	Total	A_z	Benign	Malignant	Total	A_z
A_{dg}	57.1 (16/28)	50.0 (5/10)	55.3	*	57.1 (16/28)	50.0 (5/10)	55.3	*
G_{cv}	75.0 (21/28)	50.0 (5/10)	68.4	*	75.0 (21/28)	50.0 (5/10)	68.4	*
A_{dg}, G_{cv}	67.9 (19/28)	50.0 (5/10)	63.2	0.52	75.0 (21/28)	50.0 (5/10)	68.4	0.60
GCM	78.6 (22/28)	63.6 (7/11)	74.4	0.67	82.1 (23/28)	81.8 (9/11)	82.1	0.85
A_{dg}, G_{cv}, GCM	67.9 (19/28)	30.0 (3/10)	57.9	0.5	82.1 (23/28)	50.0 (5/10)	73.7	0.84

A_{dg} —Acutance, G_{cv} —Coefficient of variation in gradient strength, GCM—Seven GCM features. A_z Area under the ROC curve. * Indicates ROC analysis was not performed for the corresponding feature set.

tained using jack-knife method were 0.67 and 0.63, respectively.

The above results support the notion that the signs of malignancy in mammographic images are concentrated more in the mass margins than in their central core portions. On the same set of images taken from the MIAS database, Rangayyan *et al.* [13] reported a benign/malignant classification accuracy of up to 75% by using various shape features. The shape features have limitations, and cannot differentiate benign and malignant masses possessing similar shapes. On the other hand, texture analysis of the information in mass margins has clearly proven to be significant and is not sensitive to the precise location of the boundaries of masses.

The differences in classification accuracies (at equal prior probabilities of the benign and malignant groups) are maintained in both the types of classification methods, thereby validating the significance of information in the mass margins. However, the jack-knife classification results show inferior trends as compared with the corresponding results obtained by using the more optimistic method of classification based on posterior probabilities. Furthermore, comparison of the A_z values of both the methods, as presented in Table I, reveals large differences in the case of results obtained using the seven most-effective GCM-based features computed from the mass margins. After a careful analysis of the results in consultation with a statistics consultant [35], we are convinced that the inferior jack-knife classification results are attributable to the restricted nature of the database used in the present study: the presence of only 11 cases in the malignant group resulted in an undesirable ratio of number of features used to the number of cases tested. The features that are short-listed, as explained at the beginning of this section, might not be effective in the jack-knife scheme with such a restricted database. However, the chosen combinations of features achieved very good results using the classification method based on posterior probabilities; the comparative trends were maintained in the results of the jack-knife method, although with reduced margins.

Part II: Margin sharpness versus textural information present in margins.

After having verified in the first part that regions extracted from mammographic mass margins carry significant information that could be used to classify masses, the second part of the analysis was focused to verify whether margins have significant sharpness information that could discriminate

benign masses from malignant tumors. From the mass margins, two gradient-based features comprising the modified measure of acutance A_{dg} and the coefficient of variation of gradient strength G_{cv} were computed for all the 54 cases in the combined database. The gradient-based values computed from a large, subtle, and highly spiculated malignant case from the MIAS database (mdb148), with approximately 9000 pixels on its boundary as identified by the radiologist involved in the present study, resulted in gross deviations from the mean values of the corresponding feature sets. This case was, therefore, treated as an outlier for the purpose of pattern classification, and discarded from further analysis. Thus, the number of malignant cases analyzed by the gradient features was limited to ten from the MIAS database, leading to a total of 25 malignant tumors in the combined database. With the trimmed database of 53 cases, the mean values of A_{dg} for the benign and malignant groups were observed to be 0.033 and 0.022, respectively; the corresponding mean values of G_{cv} were found to be 0.76 and 1.223, respectively.

To verify the applicability of the proposed gradient-based features on images taken from different databases, the analysis was initially carried out on 38 MIAS (28 benign and 10 malignant) cases and later extended to the combined database (28 benign and 25 malignant). Table II shows the benign/malignant classification accuracies obtained with the MIAS cases by using the gradient-based features (A_{dg} and G_{cv}) and Table III shows the corresponding results obtained with the combined database.

The modified acutance measure A_{dg} could obtain a classification accuracy of only 66% with the combined database in contrast to a high accuracy of 92% as reported by Rangayyan *et al.* [13] using a different version of the acutance measure: the previous definition and computation of the acutance measure has user-input parameters as explained in the section on feature extraction, which affects reproducibility. The modified measure A_{dg} in the present study has addressed all the drawbacks with the acutance measure and uses a completely automated polygonization algorithm in the computation of acutance. While it has resulted in an inferior performance, the measure is robust and the results obtained are reproducible with no user intervention.

The gradient-based features could achieve at best 68.4% accuracy only using both the classification methods with the 38 MIAS cases. In contrast, texture analysis using GCMs computed from the ribbons of pixels in mass margins provided 82.1% classification accuracy, with a jack-knife accuracy of

TABLE III
NUMBER OF CASES CORRECTLY CLASSIFIED BY THE GRADIENT-BASED AND GCM-BASED TEXTURE FEATURES COMPUTED FROM MASS MARGINS (RIBBONS)
WITH THE COMBINED DATABASE. LEGEND

Features	% Accuracy (jack-knife method)				% Accuracy			
	Benign	Malignant	Total	A_z	Benign	Malignant	Total	A_z
A_{dg}	57.1 (16/28)	76.0 (19/25)	66.0	*	57.1 (16/28)	76.0 (19/25)	66.0	*
G_{cv}	78.6 (22/28)	40.0 (10/25)	60.4	*	78.6 (22/28)	40.0 (10/25)	60.4	*
A_{dg}, G_{cv}	67.9 (19/28)	68.0 (17/25)	67.9	0.73	71.4 (20/28)	72.0 (18/25)	71.7	0.76
GCM	96.4 (27/28)	56.0 (14/25)	77.4	0.84	96.4 (27/28)	68.0 (17/25)	83.0	0.94
A_{dg}, G_{cv}, GCM	89.3 (25/28)	64.0 (16/25)	77.4	0.80	92.9 (26/28)	72.0 (18/25)	83.0	0.93

A_{dg} —Acutance, G_{cv} —Coefficient of variation in gradient strength, GCM—Seven GCM features. A_z Area under the ROC curve. * Indicates ROC analysis was not performed for the corresponding feature set.

74.4% with the 39 MIAS cases as shown in Tables I and II. This observation reveals that textural information in mass margins has better benign/malignant discriminant capabilities than sharpness information.

Gradient-based analysis applied to the combined database of 53 masses (28 benign and 25 malignant) indicated improved performance in benign/malignant classification with $A_z = 0.76$, as shown in Table III. The corresponding A_z value obtained using the jack-knife method is 0.73. It was observed that the cases that were misclassified in the analysis of the MIAS cases remained misclassified in the analysis of the combined database as well. It should be noted that the proposed gradient-based features are normalized in order to be able to use them on a mixture of databases.

Part III: Classification using combinations of gradient-based and texture-based features.

The proposed gradient-based features quantify the sharpness information in mass margins that is present in the radial direction at every point on the boundary. Such information is used by radiologists to judge the signs of malignancy. On the other hand, the GCM-based features that were found to be most effective in the benign/malignant classification of masses characterize statistical texture in mass margins and do not constitute an analysis of radial edge profiles. We performed classification tests using a combination of gradient-based and GCM-based texture features to verify if the classification trends obtained using the GCM-based features could be reinforced further by adding measures based on directional sharpness information.

The images taken from the MIAS database contain only 11 malignant cases as against 28 benign cases. Hence, a particular combination of features can assume a maximum of only nine features due to the limited degrees of freedom available for discriminant analysis with such a restricted database. The seven most-effective GCM-based texture features computed from ribbons when combined with the two gradient-based features achieved a classification accuracy of 73.7% and A_z of 0.84 under the ROC curve with 38 MIAS cases, as against an A_z of 0.6 using gradient-based measures, as shown in Table II. However, the combination achieved no better results than the seven most-effective GCM-based texture features on their own. Jack-knife classification trends, also listed in Table II, confirm the inferior performance of the combination of the two types of features. Although the reasons for the deterioration in classification accuracies are not apparent, we feel that the

addition of the less effective gradient-based features has proven to be counter-productive, and has generally brought down the discriminant capabilities of the GCM-based features.

The seven GCM-based texture features, when applied on the combined database, polarized the classification decision in favor of database groups (MIAS versus Screen Test) rather than the desired benign vs malignant classification (albeit with an accuracy of 83% and A_z of 0.94 with the corresponding jack-knife results of 77.4% and 0.84, respectively). These results, reported in Table III, do not agree well with the objective of benign/malignant classification with the combined database. This observation indicates the susceptibility of texture features to changes in contrast and spatial resolution in various databases. In the analysis of textural information in images taken from multiple databases with the intention of arriving at a common decision, as is the case in the present study, the images should be suitably normalized prior to computing the features.

VII. CONCLUSION

We have attempted to evaluate gradient and texture information possessed by mammographic masses in order to classify them as benign or malignant.

- 1) We investigated the efficacy of textural information present in mass ROIs in relation to the textural content that exists in the mass margins in ribbons of pixels around their boundaries. Texture features derived based on GCMs were used in linear discriminant analysis for benign/malignant classification. With 39 cases (28 benign and 11 malignant) selected from the MIAS database, a benign versus malignant classification accuracy of 0.85 (as indicated by the area A_z under the ROC curve) was obtained by analyzing the texture present in the mass margins. Texture analysis of mass ROIs resulted in $A_z = 0.71$. The corresponding results obtained using jack-knife classification were observed to be 0.67 and 0.63, respectively. It can be conclusively stated that analysis of texture in mass margins is effective in the discrimination of benign masses and malignant tumors. However, the results need to be verified on a larger database.
- 2) We have also proposed two gradient-based measures to evaluate the variations in sharpness information present in ribbons of pixels across the boundaries of masses. The proposed gradient-based measures were tested with 38

images selected from the MIAS database, and further applied to a combined database containing images from both the MIAS database and a local database. The measures together resulted in $A_z = 0.6$ with 38 MIAS cases and $A_z = 0.76$ with the combined database (28 benign and 25 malignant cases). The corresponding values observed using jack-knife classification were observed to be 0.52 and 0.73 for the MIAS and combined databases, respectively. The above results indicate that gradient analysis is less effective as compared to texture analysis in mass margins.

- 3) Gradient-based features when combined with GCM-based texture features computed in the mass ribbons resulted in a higher A_z of 0.84 with 38 MIAS cases, as compared to using gradient-based features alone. But the corresponding jack-knife result was observed to be poor with $A_z = 0.5$. However, texture features were found to be sensitive to the variations between the databases and could not perform the desired task of benign versus malignant discrimination on the combined database.

The ribbon used in the present work is not guaranteed to be continuous, i.e., it does not include pixels in the vicinity of the boundary that do not lie on the normals computed at the boundary points. We are developing a procedure based on morphological erosion and dilation of the boundary to extract a compact and adaptive ribbon of pixels with no holes of left-out pixels. However, the advantage of the ribbons used in the present work is that the same groups of pixels are used to compute the gradient-based and texture features.

The boundaries used in the present study were manually drawn on digitized mammograms by an expert radiologist. Recently, we have developed a mass detection algorithm [36], [37] based on multi-scale and density-variation-based principles. We are currently evaluating the effectiveness of the proposed measures to classify the mass regions as detected by our methods. We are in the process of developing a database of digitized mammograms from Screen Test: Alberta Program for the Early Detection of Breast Cancer. The proposed methods will be tested with the new database. Additionally, logistic regression methods, which do not assume multi-variate normality of the distribution of data, will be considered for pattern classification experiments. Detailed evaluation of the measures proposed with a larger database of images with consistent characteristics should provide reliable answers to the questions raised in the present study.

ACKNOWLEDGMENT

The authors thank G. Engels, Statistics Consultant, University Computing Services, University of Calgary, for her help in the pattern classification experiments.

REFERENCES

- [1] E. E. Sterns, "Relation between clinical and mammographic diagnosis of breast problems and the cancer/biopsy rate," *Can. J. Surg.*, vol. 39, no. 2, pp. 128–132, 1996.

- [2] H. C. Burrell, D. M. Sibbering, A. R. Wilson, S. E. Pinder, A. J. Evans, L. J. Yeomen, C. W. Elston, I. O. Ellis, and R. W. Blamey, "Screening interval breast cancers: Mammographic features and prognostic factors," *Radiology*, vol. 199, pp. 811–817, 1996.
- [3] M. J. Homer, *Mammographic Interpretation: A Practical Approach*. Boston, MA: McGraw-Hill, 1997.
- [4] N. R. Mudigonda, R. M. Rangayyan, and J. E. L. Desautels, "Concavity and convexity analysis of mammographic masses via an iterative segmentation algorithm," in *Proc. Can. Conf. Electrical and Computer Engineering*, M. Meng, Ed., Edmonton, AB, Canada, May 1999, pp. 1489–1494.
- [5] R. M. Rangayyan, N. R. Mudigonda, and J. E. L. Desautels, "Boundary modeling and shape analysis methods for classification of mammographic masses," *Med. Biological Eng. Comput.*, vol. 38, no. 5, pp. 487–496, 2000.
- [6] C. Kimme, B. J. O'Loughlin, and J. Sklansky, "Automatic detection of suspicious abnormalities in breast radiographs," in *Data Structures, Computer Graphics, and Pattern Recognition*, A. Klinger, K. S. Fu, and T. L. Kunii, Eds., New York: Academic, 1977, pp. 427–447.
- [7] A. Petrosian, H. P. Chan, M. A. Helvie, M. M. Goodsitt, and D. D. Adler, "Computer-aided diagnosis in mammography: classification of mass and normal tissue by texture analysis," *Phys. Med. Biol.*, vol. 39, pp. 2273–2288, 1994.
- [8] H. P. Chan, D. Wei, M. A. Helvie, B. Sahiner, D. D. Adler, M. M. Goodsitt, and N. Petrick, "Computer-aided classification of mammographic masses and normal tissue: Linear discriminant analysis in texture feature space," *Phys. Med. Biol.*, vol. 40, no. 5, pp. 857–876, 1995.
- [9] S. K. Kinoshita, P. M. A. Marques, A. F. F. Slates, H. R. C. Marana, R. J. Ferrari, and R. L. Villela, "Detection and characterization of mammographic masses by artificial neural network," in *Proc. 4th Int. Workshop Digital Mammography*, N. Karssemeijer, M. Thijssen, J. Hendriks, and L. van Erning, Eds., Nijmegen, The Netherlands, June 1998, pp. 489–490.
- [10] Z. Huo, M. L. Giger, C. J. Vyborny, U. Bick, P. Lu, D. E. Wolverton, and R. A. Schmidt, "Analysis of spiculation in the computerised classification of mammographic masses," *Med. Phys.*, vol. 22, no. 10, pp. 1569–1579, 1995.
- [11] S. L. Kok, J. M. Brady, and L. Tarassenko, "The detection of abnormalities in mammograms," in *Proc. 2nd Int. Workshop Digital Mammography*, A. G. Gale, S. M. Astley, D. R. Dance, and A. Y. Cairns, Eds., York, England, July 10–12, 1994, pp. 261–270.
- [12] D. Guliato, R. M. Rangayyan, W. A. Carnielli, J. A. Zuffo, and J. E. L. Desautels, "Segmentation of breast tumors in mammograms by fuzzy region growing," in *Proc. 20th Annu. Int. Conf. IEEE Engineering in Medicine and Biology Society*, Hong Kong, Oct. 29–Nov. 1, 1998, pp. II:1002–1004.
- [13] R. M. Rangayyan, N. M. El-Faramawy, J. E. L. Desautels, and O. A. Alim, "Measures of acutance and shape for classification of breast tumours," *IEEE Trans. Med. Imag.*, vol. 16, pp. 799–810, Dec. 1997.
- [14] W. P. Kegelmeyer, Jr., "Evaluation of stellate lesion detection in a standard mammogram data set," *Int. J. Pattern Recogn. Artif. Intell.*, vol. 7, no. 12, pp. 1477–1493, 1993.
- [15] B. R. Groshong and W. P. Kegelmeyer Jr., "Evaluation of a Hough transform method for circumscribed lesion detection," in *Proc. 3rd Int. Workshop Digital Mammography*, K. Doi, M. L. Giger, R. M. Nishikawa, and R. A. Schmidt, Eds., Chicago, IL, June 9–12, 1996, pp. 361–366.
- [16] H. Kobatake, H. Takeo, and S. Nawano, "Tumor detection system for full-digital mammography," in *Proc. 4th Int. Workshop Digital Mammography*, N. Karssemeijer, M. Thijssen, J. Hendriks, and L. van Erning, Eds., Nijmegen, The Netherlands, June 1998, pp. 87–94.
- [17] N. Petrick, H. P. Chan, D. Wei, B. Sahiner, M. A. Helvie, and D. D. Adler, "Automated detection of breast masses on mammograms using adaptive contrast enhancement and texture classification," *Med. Phys.*, vol. 23, no. 10, pp. 1685–1696, 1996.
- [18] W. E. Polakowski, D. A. Cournoyer, S. K. Rogers, M. P. DeSimio, D. W. Ruck, J. W. Hoffmeister, and R. A. Raines, "Computer-aided breast cancer detection and diagnosis of masses using difference of Gaussians and derivative-based feature saliency," *IEEE Trans. Med. Imag.*, vol. 16, pp. 811–819, Dec. 1997.
- [19] D. Brzakovic, X. M. Luo, and P. Brzakovic, "An approach to automated detection of tumours in mammograms," *IEEE Trans. Med. Imag.*, vol. 9, pp. 233–241, June 1990.
- [20] T. K. Lau and W. F. Bischof, "Automated detection of breast tumors using the asymmetry approach," *Comput. Biomed. Res.*, vol. 24, pp. 273–295, 1991.

- [21] C. E. Priebe, R. A. Lorey, D. J. Marchette, J. L. Solka, and G. W. Rogers, "Nonparametric spatio-temporal change point analysis for early detection in mammography," in *Proc. 2nd Int. Workshop Digital Mammography*, A. G. Gale, S. M. Astley, D. R. Dance, and A. Y. Cairns, Eds., York, U.K., July 10–12, 1994, pp. 111–120.
- [22] C. J. Burdett, H. G. Longbotham, M. Desai, W. B. Richardson Jr, and J. F. Stoll, "Nonlinear indicators of malignancy," in *Proc. SPIE Biomedical Image Processing and Biomedical Visualization*, vol. 1905, San Jose, CA, February 1993, pp. 853–860.
- [23] E. Claridge and J. H. Richter, "Characterization of mammographic lesions," in *Proc. 2nd Int. Workshop Digital Mammography*, A. G. Gale, S. M. Astley, D. R. Dance, and A. Y. Cairns, Eds., York, U.K., July 10–12, 1994, pp. 241–250.
- [24] B. Sahiner, H. P. Chan, N. Petrick, M. A. Helvie, and M. M. Goodsitt, "Computerized characterization of masses on mammograms: The rubber band straightening transform and texture analysis," *Med. Phys.*, vol. 25, no. 4, pp. 516–526, 1998.
- [25] M. Sameti, J. Morgan-Parkes, R. K. Ward, and B. Palcic, "Classifying image features in the last screening mammograms prior to detection of a malignant mass," in *Proc. 4th Int. Workshop Digital Mammography*, N. Karssemeijer, M. Thijssen, J. Hendriks, and L. van Erning, Eds., Nijmegen, The Netherlands, June 1998, pp. 127–134.
- [26] Y. Chitre, A. P. Dhawan, and M. Moskowitz, "Artificial neural network based classification of mammographic microcalcifications using image structure features," *Int. J. Pattern Recogn. Artif. Intell.*, vol. 7, no. 12, pp. 1377–1402, 1993.
- [27] O. Menut, R. M. Rangayyan, and J. E. L. Desautels, "Parabolic modeling and classification of breast tumours," *Int. J. Shape Modeling*, vol. 3, no. 3&4, pp. 155–166, 1998.
- [28] J. A. Ventura and J. M. Chen, "Segmentation of two-dimensional curve contours," *Pattern Recogn.*, vol. 25, no. 10, pp. 1129–1140, 1992.
- [29] H. C. Higgins and L. A. Jones, "The nature and evaluation of the sharpness of photographic images," *J. Soc. Motion Picture Television Engineers*, vol. 58, pp. 277–290, 1952.
- [30] R. M. Rangayyan and S. G. Elkadiki, "Algorithm for the computation of region-based image edge profile acutance," *J. Electron. Imag.*, vol. 4, no. 1, pp. 62–70, 1995.
- [31] J. C. Russ, *The Image Processing Handbook*. Raleigh, NC: CRC Press, 1995.
- [32] R. M. Haralick, "Statistical and structural approaches to texture," *Proc. IEEE*, vol. 67, pp. 786–804, May 1979.
- [33] J. Suckling, J. Parker, D. R. Dance, S. Astley, J. Hutt, C. R. M. Doggis, I. Ricketts, E. Stamatakis, N. Cerneaz, S. L. Kok, P. Taylor, D. Betal, and J. Savage, "The Mammographic Image Analysis Society digital mammogram database," in *Proc. 2nd Int. Workshop Digital Mammography*, A. G. Gale, S. M. Astley, D. R. Dance, and A. Y. Cairns, Eds., York, U.K., July 10–12, 1994, pp. 375–378.
- [34] M. B. Brown and L. Engelman, *BMDP Statistical Software Manual*. Berkeley, CA: Univ. California, 1988.
- [35] G. Engels, "Personal Communication," unpublished, April 2000.
- [36] N. R. Mudigonda, R. M. Rangayyan, J. E. L. Desautels, and O. Menut, "Segmentation of breast masses in mammograms: A multi-resolution and hierarchical density propagation approach," in *Proc. Computer-Assisted Radiology and Surgery*, H. U. Lemke, M. W. Vannier, K. Inamura, and A. G. Farman, Eds., Paris, France, June 1999, p. 1014.
- [37] N. R. Mudigonda, R. M. Rangayyan, and J. E. L. Desautels, "Segmentation and classification of mammographic masses," *Proc. SPIE, Vol. 3979: Medical Imaging 2000: Image Processing*, pp. 55–67, 2000.